Phonon-induced decay rates for quasiparticle cyclotron orbits in simple metals: analytical approximations and models

1993 J. Phys.: Condens. Matter 5 679

(http://iopscience.iop.org/0953-8984/5/6/005)

J. Phys.: Condens. Matter 5 (1993) 679–696. Printed in the UK

Phonon-induced decay rates for quasiparticle cyclotron orbits in simple metals: analytical approximations and models

W E Lawrence†
Department of Physics, Ohio State University, Columbus, OH 43210, USA

Received 22 June 1992, in final form 9 October 1992

Abstract. A formalism is developed for studying the temperature dependence of phonon-induced quasiparticle scattering rates averaged over cyclotron orbits in simple metals. The underlying model is expressed in terms of analytic forms for the spectral distribution $\alpha^2F(\omega)$, from which the scattering rate $\tau^{-1}(T)$ is easily computed. The material-dependent parameters upon which the results depend are the inter-sheet threshold wavevector Q_1, orbit caliper Q_2, transverse and longitudinal sound velocities c_T and c_L, and a parameter R expressing the importance of the momentum dependence of the pseudopotential form factor, all of which are known in many cases. The orbitally averaged scattering rates exhibit a regime of T^2 dependence that is not associated with individual point rates, above a characteristic temperature $T_1 \sim Q_1 c_T$.

1. Introduction

Theoretical treatments of the electron–phonon interaction range from the very simple, as in the jellium model, to the very complex, involving detailed computations of the band structure and phonon spectra (see for example Pickett 1989, ch X). An intermediate level of treatment was developed for the electrical resistivity (Lawrence and Wilkins 1972) (LW), and also applied to quasiparticle scattering rates τ^{-1} (Wagner and Bowers 1978) (WB). At this level one finds analytical formulae for the scattering rates, for example, which exhibit qualitatively different behaviour from that of the jellium model. Instead of an isotropic T^3 dependence, one finds enormous anisotropy, with T^3 dependence guaranteed only at very low temperatures; departures may set in at temperatures as low as 1 K or so.

The purpose of this paper is to apply the same level of treatment to orbital averages of scattering rates, as measured in the radiofrequency size effect (RFSE) (see a current review by Gasparov and Huguenin (1992)), and to show in detail how the temperature dependence relates to the geometry of the orbit. Among other things, we will explore the temperature regime over which the T^2 contribution‡ predicted by Lawrence *et al* (1986) (LCS) should be detectable. While the anisotropy has been found in many experiments, such departures from T^3 dependence attributable to the electron–phonon contribution have only been seen in recent RFSE data (Probst *et al* 1980, Jaquier *et al* 1991).

† Permanent address: Department of Physics, Dartmouth College, Hanover, NH 03755, USA.

‡ This electron–phonon T^2 contribution is distinguishable from the electron–electron one by its limited temperature regime and its anisotropy, as discussed by Jaquier *et al* (1991).

0953-8984/93/060679+18$07.50

It is convenient to describe the present treatment in terms of the spectral density function $\alpha^2F(\omega)$. In these terms, the decay rate of a quasiparticle in the state k on the Fermi surface (e.g. WB, equation (2.24)) may be written as

$$\tau^{-1}(k,T) = 4\pi \int_0^\infty d\omega\, \alpha^2F(k,\omega)[\sinh(\hbar\omega/k_BT)]^{-1} \tag{1.1}$$

where

$$\alpha^2F(k,\omega) = (2\pi)^{-3} \int \frac{dS'}{\hbar v'} \sum_\sigma |g^\sigma_{kk'}|^2 \delta(\omega - \omega_{q\sigma}) \tag{1.2}$$

is the effective density of phonon states for scattering an electron from state k, and

$$|g^\sigma_{kk'}|^2 = (2\rho\omega_{q\sigma})^{-1}|M^\sigma_{kk'}|^2 \tag{1.3}$$

$$M^\sigma_{kk'} = (1/i)\hat{\epsilon}_{q\sigma} \cdot \langle \psi_{k'}|\nabla V|\psi_k\rangle \tag{1.4}$$

is the squared matrix element for scattering by absorption (emission) of a phonon with wavevector $\pm q = k' - k$, frequency $\omega_{q\sigma}$ and polarization $\hat{\epsilon}_{q\sigma}$. The integral in equation (1.2) is over the Fermi surface, and ρ is the mass density of the metal.

The definition (1.1) applies to orbital averages Γ as well as to points k. The appropriate orbital average (for either τ^{-1} or α^2F) is

$$f(\Gamma) = \oint \frac{dk}{v} f(k) \left(\oint \frac{dk}{v} \right)^{-1} \tag{1.5}$$

where $v = v(k)$ is the unrenormalized or 'band' velocity. The renormalization of the decay rate (due principally to the electron–phonon interaction) is accounted for by

$$\tau_{ren}(k) = \tau_{bare}(k)[1 + \lambda(k)]$$

and of its orbital average by

$$\tau_{ren}(\Gamma) = \tau_{bare}(\Gamma)[1 + \lambda(\Gamma)] \tag{1.6}$$

where $\lambda(\Gamma)$ and $\lambda(k)$ are related by equation (1.5). Since in fact $\lambda(k)$ is relatively isotropic, the Fermi-surface averages tabulated by Grimvall (1976) usually suffice.

As stated, equation (1.1) refers to the scattering rate evaluated at the Fermi energy. In the experimental data, complications may arise from the energy dependence of τ^{-1} or from reduced scattering 'effectiveness', depending upon experimental parameters such as the radiation frequency and the sample thickness. These matters have been dealt with successfully by Stubi *et al* (1988), and we shall not be concerned with them here.

1.1. Characteristic dimensions and regimes

This paper is organized by defining the regime of T^2 behaviour in terms of orbit dimensions. Since the T^2 dependence arises from Umklapp scattering between free-electron-like regions of the Fermi surface, its regime is limited below by the continuity of the Fermi surface at zone boundaries (the essential band-structure effect), which guarantees that $\tau^{-1} \sim T^3$ as $T \to 0$. The crossover is determined by a characteristic wavevector Q_1 that defines the scale of Fermi-surface distortions near the zone boundary (G). For definiteness we take this to be the 'inter-sheet threshold' pictured in figure 1,

$$Q_1(G) = \frac{2|V(G)|}{\hbar v_\perp} = \frac{2m|V(G)|}{\hbar^2 k_F \sin \chi_G} \tag{1.7}$$

where $V(G)$ is the effective pseudopotential parameter in a two orthogonalized plane-waves (2-OPW) description of local Fermi-surface shape and $v_\perp$ is the Fermi velocity at the zone boundary intersection. χ_G is half the vertex angle of the orbit.

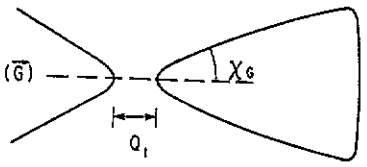

Figure 1. Threshold wavevector Q_1 for inter-sheet scattering near a vertex.

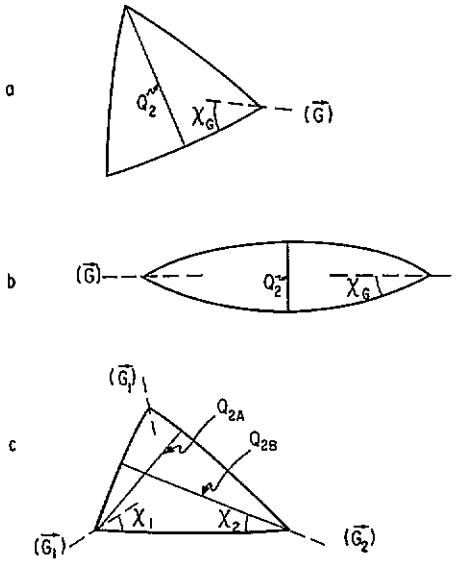

Figure 2. Minimum calipers Q_2 for (a) equilateral triangle, (b) lens and (c) isosceles triangle. In (c), Q_{2A} and Q_{2B} apply to the two legs attached to the upper (G_1) vertex.

The quadratic regime is limited *above* by a cusp in the Umklapp scattering phase space. As shown in the next section and pictured in figure 2, this cusp occurs at a minimum caliper Q_2 of the orbit; for example, the width of a lens or the height(s) of a triangle. In the case of an isosceles triangle, there are two Q_1 and two Q_2 values. In the absence of such multiplicities, there are three regimes separated by the two characteristic wavevectors, Q_1 and Q_2, or the corresponding frequencies or temperatures

$$k_B T_i = \hbar \Omega_i = \hbar c_T Q_i \qquad (i = 1,2) \tag{1.8}$$

where c_T is a transverse sound velocity. The three characteristic frequency dependences, to be derived in the next two sections, are roughly $\alpha^2F(\Gamma,\omega) \sim \omega^2 \sim \omega$ and ~ 1 for low, intermediate and high frequencies, respectively. The high-frequency regime is interesting only because it limits the intermediate regime. In orbits with multiple Q_1 and Q_2 values, $\alpha^2F(\Gamma,\omega)$ is a superposition of contributions with overlapping regimes.

In the next section we discuss the intermediate and high-frequency regimes (and derive Q_2) by using the 1-OPW model and ignoring Fermi-surface distortions near zone boundaries (except insofar as they define the orbit). The 2-OPW model is then introduced in section 3 to discuss the low-frequency regime and complete the construction of a model α^2F function. Corrections to this basic model are discussed in section 4, and representative results shown in section 5.

2. One orthogonalized plane-wave treatment and Ω_2

The main result of this treatment has already been presented in LCS for the case of triangular orbits in Cd. We review and generalize this result in the α^2F language. The matrix elements for normal and Umklapp scattering are, respectively,

$$M^{\sigma}_{kk'} = \hat{\epsilon}_{q\sigma} \cdot qV(q) \tag{2.1a}$$

$$M^{\sigma}_{kk'} = \hat{\epsilon}_{q\sigma} \cdot (q+G)V(q+G) \tag{2.1b}$$

where $q \equiv k' - k$ is the phonon wavevector (reduced to the first Brillouin zone in the Umklapp case), $V(q)$ may be set to $V(0)$, and we temporarily set $V(q+G) \to V(G)$. Corrections to the latter may be significant, and these are taken up in section 4.

If the initial state k is sufficiently close to a zone boundary, then the final-state integration for $\alpha^2F(k,\omega)$ traces out two circular regions (normal and Umklapp, as shown in figure 3), and α^2F is the sum of

$$\alpha^2F_N(k,\omega) = (8\pi^2\hbar\rho v_F)^{-1}V^2(0)\omega^2/c_L^4 \tag{2.2a}$$

and

$$\begin{aligned}\alpha^2F_U(k,\omega) = (8\pi^2\hbar\rho v_F)^{-1}&G^2V^2(G)(1+q_0/k_F)^{-1}\\ &\times \tfrac{1}{2}\{c_L^{-2}\theta(\omega - c_Lq_0)[\sin^2\chi_G + (c_Lq_0/\omega)^2\cos(2\chi_G)]\\ &+ c_T^{-2}\theta(\omega - c_Tq_0)[1+\cos^2\chi_G - (c_Tq_0/\omega)^2\cos(2\chi_G)]\}.\end{aligned} \tag{2.2b}$$

The normal contribution is from longitudinal phonons only, as dictated by equation (2.1*a*). The Umklapp contribution vanishes for $\omega < c_Tq_0$, where the 'Umklapp threshold' q_0 is the distance from k to the remapped sphere. The derivation of the full expression (2.2*b*) is straightforward and too lengthy to present here†. The presence of the step discontinuities is a purely geometrical effect. The q_0/k_F term gives the Fermi-surface curvature correction to the density of final states for Umklapp

† Available from the author at the permanent address listed are details of derivations not presented in the text, series expressions for the scattering rate, and computer code to evaluate these expressions.

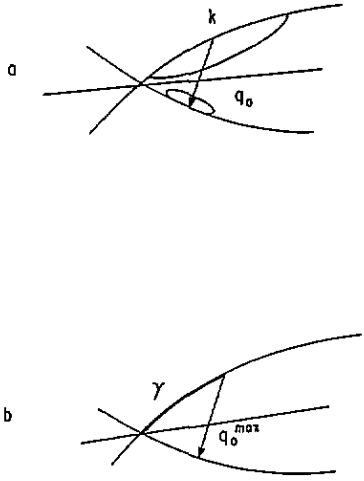

Figure 3. (*a*) Circular regions of normal and Umklapp contributions to $\alpha^2F(k,\omega)$ for $\omega > cq_0$, and (*b*) orbit segment γ, showing maximum Umklapp threshold on the segment.

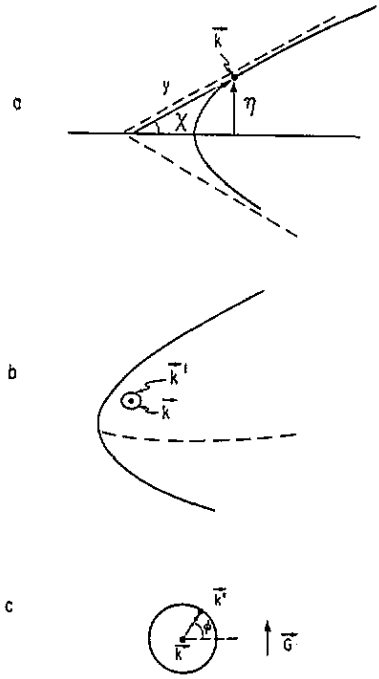

Figure 4. Geometry for 2-OPW treatment at low ω: (*a*) dimensionless variable η for Fermi-surface point k; (*b*) and (*c*) locus of final states k' is circular for $\omega \to 0$.

scattering. This term may be dropped since it is unimportant compared with other corrections that will be calculated in section 4. Note that the Umklapp term simplifies, if $c_L = c_T \equiv c$, to

$$\alpha^2F_U(k,\omega) = (8\pi^2\hbar\rho v_F c^2)^{-1}G^2V^2(G)\theta(\omega - cq_0). \tag{2.3}$$

Let us proceed with this simplification, and generalize at the end of this section.

The average of equation (2.3) over an orbit segment γ that touches the zone boundary (see figure 3(*b*)) is equivalent to the average over q_0 values in $0 < q_0^{max}$:

$$\alpha^2F_U(\gamma,\omega) = (8\pi^2\hbar\rho v_F c^3 q_0^{max})^{-1}G^2V^2(G)\min(\omega, cq_0^{max}). \tag{2.4}$$

Orbit averages for the orbit types shown in figure 2 may be constructed from this expression. The lens average is identical to that of its irreducible quarter segment, with $q_0^{max} = Q_2$ the width of the lens. The equilateral-triangle average is equal to that of its irreducible one-sixth segment, although the naive application of equation (2.4) to this segment gives the wrong results if one fails to account for the presence of two zone boundaries across which Umklapp can occur from each point, one with $0 < q_0 < \frac{1}{2}Q_2$ and the other with $\frac{1}{2}Q_2 < q_0 < Q_2$. It is much simpler to apply equation (2.4) to an entire leg (where clearly $0 < q_0 < Q_2$ for both of the relevant zone bondaries), and to double the expression to account for the two kinds of Umklapp. So the orbit averages for the equilateral triangle (ET) and lens are

$$\alpha^2F_U(\Gamma,\omega) = \binom{2}{1}(8\pi^2\hbar\rho v_F c^3 Q_2)^{-1}G^2V^2(G)\min(\omega, cQ_2) \qquad \begin{cases} \text{ET} \\ \text{lens} \end{cases} \tag{2.5}$$

where Q_2 is defined for each orbit in figure 2. The isosceles-triangle average may be computed as the sum of leg averages, each weighted by the ratio of leg length Q_γ to total orbit length (or perimeter) Q_Γ. Each leg average is the sum of two expressions of the type (2.4) in which different Q_2 values may appear. Formally,

$$\alpha^2 F_U(\Gamma) = \sum_\gamma \frac{Q_\gamma}{Q_\Gamma} \sum_{G(\gamma)} \frac{1}{Q_2} \min(\omega, cQ_2) g(G)$$

where γ is the leg index, the interior sum is over the two vertices attached to the leg γ, and $g(G)$ is the full expression (2.4) for $\alpha^2 F(\gamma)$ except for the Q_2- (or q_0^{max})-dependent factors that are made explicit. Now according to figure 2, $(Q_\gamma/Q_2) = \operatorname{cosec}(2\chi_G)$ depends only on the vertex, so that we may switch the order of summation and write

$$\alpha^2 F_U(\Gamma) = \frac{1}{Q_\Gamma} \sum_G \operatorname{cosec}(2\chi_G) g(G) \sum_{\gamma(G)} \min(\omega, cQ_2).$$

The interior sum is over the two legs attached to the vertex G, for which Q_2 may take on different values, as in the isosceles triangle (IT) G_1 vertices. With the exception of a single equation, we shall not be concerned with such cases in this paper. Therefore we drop the γ sum and multiply by 2, with the understanding that the function $\min(\omega, cQ_2)$ would be averaged over the two values of Q_2 if these were different. The result for any orbit is then simply

$$\alpha^2 F_U(\Gamma, \omega) = 2(8\pi^2 \hbar \rho v_F c^3 Q_\Gamma)^{-1} \sum_G \operatorname{cosec}(2\chi_G) G^2 V^2(G) \min(\omega, cQ_2). \tag{2.6}$$

Now to dispose of the single exception, we apply equation (2.6) to the isosceles triangle of figure 2, with the result

$$\begin{aligned}\alpha^2 F_U(\Gamma, \omega) = 2(8\pi^2 \hbar \rho v_F c^3 Q_\Gamma)^{-1} \{ & \operatorname{cosec}(2\chi_1) G_1^2 V^2(G_1) [\min(\omega, cQ_{2A}) \\ & + \min(\omega, cQ_{2B})] + \operatorname{cosec}(2\chi_2) G_2^2 V^2(G_2) \min(\omega, cQ_{2A})\}\end{aligned} \qquad \text{IT.} \tag{2.7}$$

As a final consistency check, we may recover the equilateral-triangle and lens cases trivially from equation (2.6) in the form

$$\alpha^2 F_U(\Gamma, \omega) = \binom{6}{4} (8\pi^2 \hbar \rho v_F c^3 Q_\Gamma)^{-1} \operatorname{cosec}(2\chi_2) G^2 V^2(G) \min(\omega, cQ_2) \qquad \begin{cases} \text{ET} \\ \text{lens.} \end{cases} \tag{2.8}$$

Clearly the ET result is a special case of equations (2.6) and (2.7), but it is also equivalent to equation (2.5) since $Q_\Gamma = 3Q_\gamma = 3Q_2 \operatorname{cosec}(2\chi_G)$. The lens cases of equations (2.8) and (2.5) are also equivalent in the limit where $Q_2 \ll k_F$, although for the lens geometry this requires small χ so that $\operatorname{cosec}(2\chi) \simeq (2\chi)^{-1}$. To the extent that curvature corrections enter, the last equation (2.8) is the correct one at

low ω, with frequency-dependent corrections expressed by the (unimportant) q_0/k_F term in equation (2.2*b*).

The corresponding orbitally averaged decay rates are given by series expansions (LCS, equation (8)), which reduce to simple analytical forms far above or below T_2. The low-temperature form corresponding to equation (2.8) is

$$\tau_U^{-1}(\Gamma,T) \to \left.\frac{\partial\alpha^2F(\Gamma,\omega)}{\partial\omega}\right|_{\omega<\Omega_2} \pi^3(k_B/\hbar)^2$$
$$= 2\pi(8\hbar\rho v_F c^3 Q_\Gamma)^{-1}(k_B T/\hbar)^2 \sum_G [\operatorname{cosec}(2\chi_G)]G^2V^2(G). \tag{2.9}$$

Far above T_2 a linear dependence is approached.

For the more general case $c_L \neq c_T$ we reconsider the q_0 average leading from the point α^2F function (equation (2.2*b*)) to its orbit averages (equation (2.4)). For $\omega < c_T Q_2$, remarkably, the χ_G-dependent terms again disappear, resulting in equation (2.4) but with the replacement

$$c^{-3} \to \tfrac{2}{3}c_T^{-3} + \tfrac{1}{3}c_L^{-3} \qquad (\omega < c_T Q_2).$$

For $\omega > c_T Q_2$ there is a small additional frequency-dependent correction, which vanishes at $\omega = c_T Q_2$. This has negligible effect on τ^{-1} in the regime $T \lesssim T_2$, which applies to the experimental results, and so we ignore it. The general result for $\alpha^2F(\Gamma,\omega)$ incorporating the upper crossover is thus given by equation (2.4) with

$$c^{-3}\min(\omega, cQ_2) \to \tfrac{2}{3}c_T^{-3}\min(\omega, c_T Q_2) + \tfrac{1}{3}c_L^{-3}\min(\omega, c_L Q_2). \tag{2.10}$$

Since $c_T \lesssim \frac{1}{2}c_L$ typically, the transverse contributions to $\alpha^2F_U(\Gamma,\omega)$ and to $\tau_U^{-1}(\Gamma,T)$ dominate the longitudinal by about an order of magnitude; longitudinal phonons contribute essentially only through normal processes.

3. Two orthogonalized plane-waves treatment and Ω_1

The smoothing of cusps at zone boundaries converts the ω dependence of $\alpha^2F_U(\Gamma,\omega)$ to ω^2 dependence in the limit $\omega \to 0$, with the characteristic crossover frequency $\Omega_1 = c_T Q_1$ determined by the scale of Fermi-surface distortion. The 2-OPW model provides a simple expression for the coefficient of ω^2.

The state ψ_k is described near a zone boundary (G) by mixing coefficients α and β for 1-OPW states k and $k-G$, respectively. The matrix element (equation (1.4)) becomes

$$M^\sigma_{kk'} = \hat{e}_{q\sigma}\cdot[qV(0)(\alpha'\alpha+\beta'\beta) + (q-G)V(q-G)\beta'\alpha$$
$$+ (q+G)V(q+G)\alpha'\beta] \tag{3.1}$$

and the 1-OPW expressions (equations (2.1*a*, *b*)) are recovered from this when k and k' are far removed from zone boundaries, where the mixing coefficient factors approach either zero or unity ($\alpha'\alpha + \beta'\beta$ to select normal geometry and the other to select

Umklapp). In fact $\alpha'\alpha+\beta'\beta$ also approaches unity *near* zone boundaries in the limit $q \to 0$, indicating that the contribution to α^2F from longitudinal phonons (arising almost exclusively from the $V(0)$ term in equation (3.1)) is not changed substantially by band-structure effects at small ω. The corresponding contribution to τ^{-1} is thus $\sim T^3$ (and $\sim c_L^{-4}$) over the entire temperature range of interest.

Accordingly, we may focus on the other terms, which contribute almost exclusively through transverse phonons, and which survive far from zone boundaries only in the Umklapp geometry. The important terms in a Taylor expansion in the explicit q dependence are

$$M^{\sigma}_{kk'} = \hat{\epsilon}_{q\sigma} \cdot [GV(G)(\alpha'\beta - \beta'\alpha) + G(q \cdot G)V'(G)(\alpha'\beta + \beta'\alpha)]. \tag{3.2}$$

Both terms lead to a linear q dependence for $M^{\sigma}_{kk'}$ in the limit of small q (which in turn leads to $\alpha^2F \sim \omega^2$). For a fixed (and small) value of $q = |k' - k|$, the mixing coefficient factors are sharply peaked for k (and k') near the zone boundary, and drop to zero as they move away. It is therefore convenient to express these factors in terms of a dimensionless 'distance' from the zone boundary (figure 4(*a*)) as was introduced by LW:

$$\eta = \hbar^2 G \cdot (k - \tfrac{1}{2}G)[2m|V(G)|]^{-1}. \tag{3.3}$$

Keeping just the leading term $\sim O[V(G)]$ in equation (3.2) for now, this leads to $\lim_{q\to 0}(\alpha'\beta - \beta'\alpha) = \hbar^2 q \cdot G[4mV(G)(\eta^2+1)]^{-1}$ and hence

$$\lim_{q\to 0} M^{\alpha}_{kk'} = \hbar^2(\hat{\epsilon}_{q\sigma} \cdot G)(q \cdot G)[4m(\eta^2+1)]^{-1} \tag{3.4}$$

whose maximum value (at $\eta = 0$) is, remarkably, independent of $V(G)$, a point noted by LW and WB. The cancellation of the $V(G)$ factor at the zone boundary is caused by the rapid variation of mixing coefficients [note that $\alpha'\beta - \beta'\alpha \simeq (k'_G - k_G)\beta^2\partial(\alpha/\beta)/\partial k_G$]. The point-dependent $\alpha^2F(k,\omega)$ reduces at small ω to a circular average in the plane of the Fermi surface at k (figures 4(*b*) and (*c*)). Keeping just the transverse modes, we have

$$\sum_T (\epsilon_{q\sigma} \cdot G)^2 = G^2[1 - (\hat{q} \cdot \hat{G})^2]$$

and

$$\lim_{\omega\to 0} \alpha^2F(k,\omega) = (8\pi^2\hbar\rho v(k)c_T^4)^{-1}\omega^2 \langle (q \cdot G)^2 - (q \cdot G)^4 \rangle_{\phi} \times (\hbar^2G^2/4m)^2(\eta^2+1)^{-2}. \tag{3.5}$$

Let us make explicit the η dependences of the velocity and the circular averages:

$$v(k) = v_F(\eta^2 + \sin^2\chi)^{1/2}(\eta^2+1)^{-1/2} \tag{3.6a}$$

$$\langle (\hat{q} \cdot G)^2 \rangle_{\phi} = \tfrac{1}{2}\sin^2\chi(\eta^2+1)(\eta^2+\sin^2\chi)^{-1} = \tfrac{1}{2}(1+y^2\sin^2\chi)(1+y^2)^{-1} \tag{3.6b}$$

$$\langle (\hat{q} \cdot \hat{G})^4 \rangle_{\phi} = \tfrac{3}{8}(1+y^2\sin^2\chi)^2(1+y^2)^{-2} \tag{3.6c}$$

where the trivial rescaling (note figure 4(*a*))

$$\eta \equiv y \sin \chi \tag{3.7}$$

will simplify some of the expressions. The velocity achieves its minimum value $v_F \sin \chi$ at the zone boundary and approaches v_F at large $|\eta|$. The angular average factor in equation (3.5) is equal to 1/8 at $\eta = y = 0$, and may increase or decrease slightly at non-zero η, depending upon the value of χ. Equation (3.5) now becomes

$$\lim_{\omega \to 0} \alpha^2 F(\boldsymbol{k}, \omega) = (8\pi^2 \hbar \rho v_F c_T^4)^{-1} \omega^2 \sum_G (\hbar^2 G^2/8m)^2 [2 \sin \chi_G \times (1 + y^2)^{5/2} (1 + y^2 \sin^2 \chi_G)^{1/2}]^{-1} [1 + y^2 (4 - 3 \sin^2 \chi_G)]. \tag{3.8}$$

This in turn leads to the asymptotic cubic dependence of the point scattering rate

$$\lim_{T \to 0} \tau^{-1}(\boldsymbol{k}, T) = \left. \frac{\partial^2 (\alpha^2 F(\boldsymbol{k}, \omega))}{\partial \omega^2} \right|_{\omega = 0} 7\pi \zeta(3) (k_B T/\hbar)^3. \tag{3.9}$$

As noted by WB, the maximum value of τ^{-1}, achieved at the zone boundary, is independent of $V(G)$, and is at least an order of magnitude larger than the (approximately isotropic) normal contribution, obtained from equation (2.2*a*).

The orbital average of equation (3.8) or (3.9) may be expressed as a sum of y integrals, one for each intersected zone boundary. Making a separate transformation near each intersection,

$$\int \frac{\mathrm{d}k}{v(k)} = \frac{1}{v(y=0)} \int \mathrm{d}(\boldsymbol{k} \cdot \hat{\boldsymbol{G}}) = \frac{2m|V(G)|}{v_F \hbar^2 G} \int \mathrm{d}y \tag{3.10}$$

where equations (3.3), (3.6*a*) and (3.7) were used, we find

$$\lim_{\omega \to 0} \alpha^2 F(\Gamma, \omega) = (8\pi^2 \hbar \rho v_F c_T^4 Q_\Gamma)^{-1} \omega^2 \sum_G (\hbar^2 G^3/16m) |V(G)| I_G^{(0)} \operatorname{cosec} \chi_G \tag{3.11}$$

where the integral $I_G^{(0)}$ is of order unity and only weakly dependent on χ_G since we have factored out the main dependence ($\operatorname{cosec} \chi_G$). In particular, $I_G^{(0)}$ is a special case of

$$I_G^{(n)} = \int \mathrm{d}y \frac{(1 + y^2 \sin^2 \chi_G)^{(n-1)/2}}{4(1 + y^2)^{5/2}} [1 + y^2 (4 - 3 \sin^2 \chi_G)] \tag{3.12}$$

that will be useful later. Typical values are listed in table 1. Again, $\tau^{-1}(\Gamma, T)$ is obtained from equation (3.11) by an equation like (3.9). Comparison of equations (3.8) and (3.11) shows that the local maxima of $\tau^{-1}(\boldsymbol{k}, T)$ near zone boundaries have widths proportional to $|V(G)|$, as expected.

The separation into distinct zone boundary intersection regions is valid as long as Q_1 and Q_2 are not too close, because the integrand falls rapidly to zero with increasing $|y|$. By the same token, the limits of integration of I_G may be taken as $\pm\infty$.

Table 1. Geometrical parameters a (equation (3.14)), b (equation (4.10)) and α_2 (equation (4.3*b*)) and integrals $I_G^{(n)}$ (equation (3.12)) for typical values of the vertex half-angle χ. Corrections to a from the momentum dependence of the pseudopotential are given by equation (4.8).

χ (deg)	a	b	α_2	$I_G^{(0)}$	$I_G^{(1)}$	$I_G^{(2)}$
25	0.87	1.8	0.27	0.79	0.91	1.16
30	1.2	2.2	0.375(3/8)	0.74	0.875(7/8)	1.18
35	1.7	2.5	0.49	0.69	0.84	1.18
40	2.3	2.8	0.62	0.64	0.79	1.17

Having now exhausted the regimes in which reasonable analytical approximations can be obtained, we construct a model for the $\omega \sim \Omega_1$ region by interpolating in the manner of LW. Here, $\alpha^2F(\Gamma,\omega)$ is the appropriate vehicle; we assume that it comprises equal parts interband and intraband contributions for $\omega > \Omega_1$, that the interband cuts off abruptly below Ω_1, and that the remaining intraband contribution is the lesser of the two asymptotic forms, i.e. equation (3.11) at lower frequencies and equation (2.6) above. The resulting function is plotted in figure 5 and may be written formally as

$$\alpha^2F(\Gamma,\omega) = \tfrac{2}{3}(8\pi^2\hbar\rho v_F c_T^3 Q_\Gamma)^{-1}\sum_G \operatorname{cosec}(2\chi_G)G^2V^2(G)[\theta(\omega-\Omega_1)\min(\omega,\Omega_2) + \min(\omega^2/a\Omega_1,\omega,\Omega_2)] \tag{3.13}$$

where $\min(\alpha,\beta,\gamma)$ takes the values of its smallest argument (as a function of ω) and $a\Omega_1$ is the intraband crossover frequency, with

$$a = 4\sin\chi_G(3I_G^{(0)}\cos^2\chi_G)^{-1} \tag{3.14}$$

of order unity. In figure 5 this is set to 1.2, appropriate for an equilateral-triangle orbit where $\chi = 30°$ (table 1). In the general case, Ω_1 (and a) may depend upon G, and Ω_2 may depend upon both G and the leg attached to the vertex. In such cases the 'min' functions must be averaged over the two 'leg' values of Ω_2, as in equation (2.6).

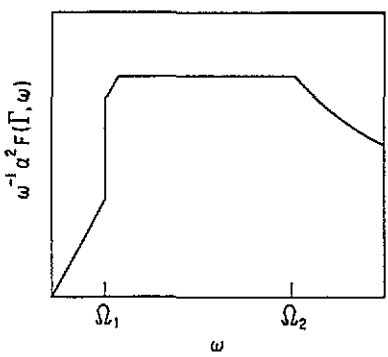

Figure 5. The interpolated $\alpha^2F(\Gamma,\omega)$ function showing (schematically) the interband cut-off at $\omega = \Omega_1$, the intraband crossover at frequencies slightly above Ω_1, and the cusp in Umklapp phase space at Ω_2.

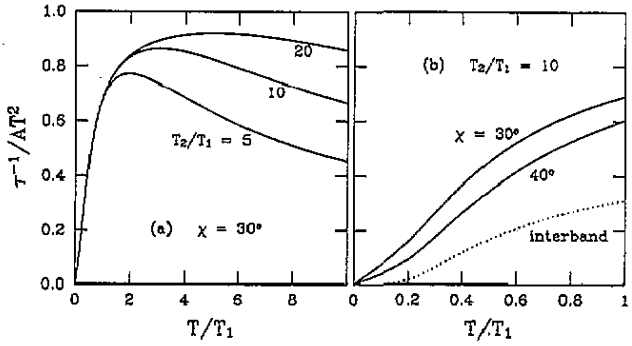

Figure 6. Scattering rate normalized to the asymptotic form AT^2 (equation (3.15)) showing (*a*) its approximate quadratic dependence for $T > T_1$ and (*b*) its cubic and exponential dependences for $T < T_1$. The dotted curve indicates the interband contribution to both full curves in (*b*). The curves in (*b*) are almost unaffected by the choice of T_2/T_1, and those in (*a*) depend little on the choice of χ for $T > T_1$.

The resulting temperature dependence of the orbitally averaged scattering rate $\tau^{-1}(\Gamma, T)$ is shown in figure 6(*a*) for a variety of ratios T_2/T_1 $(= \Omega_2/\Omega_1)$ to demonstrate the existence of the intermediate regime in which $\tau^{-1} \sim T^2$. The plot is made with reference to a nominal T^2 coefficient A, which is defined by the asymptotic limit

$$AT^2 \equiv \lim_{\substack{T_1 \to 0 \\ T_2 \to \infty}} \tau^{-1}(\Gamma, T) = \frac{\partial \alpha^2 F(\Gamma, \omega)}{\partial \omega}\Big|_{\Omega_1 < \omega < \Omega_2} \pi^3 (k_B T/\hbar)^2$$

$$= \tfrac{4}{3}\pi N_G (8\hbar\rho v_F c_T^3 Q_\Gamma)^{-1} \operatorname{cosec}(2\chi_G) G^2 V^2(G) (k_B T/\hbar)^2 \qquad (3.15)$$

where N_G is the number of vertices, assumed equivalent for plotting purposes. This expression is consistent with equations (2.9) and (2.10) since we are counting only transverse phonons here.

Regarding the low-temperature regime, figure 6(*b*) shows that the exponential onset of the inter-sheet Umklapp contribution may or may not be apparent, depending on the value of χ through the intraband crossover parameter a (equation (3.14) and table 1). The T^3 asymptote approached as $T \to 0$ is given by a combination of equations (3.9) and (3.11).

Although this clearly suggests that a T^2 regime should be observable experimentally, more quantitative discussion should be deferred until after corrections are taken into account.

4. Corrections due to $V'(G)$

Corrections due to the momentum dependence of the form factor are relatively unimportant in the low-temperature limit, where they simply increase the coefficient of T^3 somewhat, but potentially very important for $T > T_1$, because they contribute here as T^4 or T^3 and therefore may change the shape of $\tau^{-1}(\Gamma, T)$. Therefore let us first address the $T > T_1$ regime with a 1-OPW treatment parallel to that of section 2.

The desired matrix element is obtained by considering equation (3.1) far from zone boundaries in the Umklapp geometry, where it reduces to equation (3.2) with mixing coefficient factors set to unity. Again counting only transverse phonons,

$$\sum_T |M^\sigma_{kk'}|^2 = \sum_T |\hat{\epsilon}_{q\sigma} \cdot \boldsymbol{G}|^2 |V(\boldsymbol{G}) + (\boldsymbol{q} \cdot \hat{\boldsymbol{G}}) V'(\boldsymbol{G})|^2$$

$$= (1 - x^2) G^2 \{V^2(\boldsymbol{G}) + 2qxV(\boldsymbol{G})V'(\boldsymbol{G}) + q^2 x^2 [V'(\boldsymbol{G})]^2\} \tag{4.1}$$

where $x \equiv (\hat{\boldsymbol{q}} \cdot \hat{\boldsymbol{G}})$. To obtain the point $\alpha^2 F(\boldsymbol{k}, \omega)$ function, we integrate over the Umklapp circular region in figure 3, with results similar to equation (2.2*b*) but considerably more complicated. These results must then be averaged over an orbit segment γ to obtain $\alpha^2 F(\gamma, \omega)$. The details will not be presented here†. The important points are that the cross-term, being an odd function of x, has a small (though non-vanishing) angular average, and contributes much less than the other terms for all ω (and T). The remaining correction term, when averaged over an orbit segment γ, again has a remarkably simple form for $\omega < \Omega_2$, although not so simple above this. The result, denoting corrections by the prefix δ, is

$$\delta\alpha^2 F(\gamma, \omega) = \tfrac{2}{15}(8\pi^2 \hbar \rho v_F c_T^5 Q_2)^{-1} G^2 [V'(\boldsymbol{G})]^2 \min[\omega^3, p(\omega)] \tag{4.2}$$

where

$$p(\omega) = \alpha_2 \Omega_2 \omega^2 + \alpha_0 \Omega_2^3 \tag{4.3a}$$

$$\alpha_2 = \tfrac{3}{2} \sin^2 \chi_G = 1 - \alpha_0 \tag{4.3b}$$

so that the crossover from ω^3 to the second-degree polynomial $p(\omega)$ occurs at $\omega = \Omega_2$. As before, $\Omega_2 / c_T = Q_2 = q_0^{\max}$ in figure 3(*b*).

The $\omega > \Omega_2$ behaviour has been simplified, in keeping with the treatment of section 2, by using the functional form associated with the full Debye approximation $c_L = c_T$. This simplifies α_2 and α_0, and eliminates an unimportant correction term, which vanishes at $\omega = \Omega_2$.

The generalization of equation (4.2) to a full orbit average in the form of equation (2.6) is

$$\delta\alpha^2 F(\Gamma, \omega) = \tfrac{4}{15}(8\pi^2 \hbar \rho v_F c_T^5 Q_\Gamma)^{-1} \sum_G \operatorname{cosec}(2\chi_G) G^2 [V'(\boldsymbol{G})]^2 \min[\omega^3, p(\omega)]. \tag{4.4}$$

It is understood that the min function is to be averaged over the two Ω_2 values, if these differ.

For the low-ω limit, let us return to equation (3.2) and consider the correction term $\delta M^\sigma_{kk'}$. In the limit as $q \to 0$, we have $(\alpha'\beta + \beta'\alpha) \to \pm \operatorname{sgn}(V(\boldsymbol{G}))(\eta^2 + 1)^{-1/2}$ (independent of q), where η is defined by equation (3.3) and $\pm$ refers to the upper (lower) of the two bands split by $V(\boldsymbol{G})$. The resulting correction to equation (3.4) is

$$\lim_{q \to 0} \delta M^\sigma_{kk'} = \pm \operatorname{sgn}(V(\boldsymbol{G}))(\hat{\epsilon}_{q\sigma} \cdot \hat{\boldsymbol{G}})(\boldsymbol{q} \cdot \boldsymbol{G}) V'(\boldsymbol{G})(\eta^2 + 1)^{-1/2}. \tag{4.5}$$

† Available from the author at the permanent address listed are details of derivations not presented in the text, series expressions for the scattering rate, and computer code to evaluate these expressions.

The angular dependences of M and δM are identical; their ratio is simply

$$\lim_{q\to 0}(\delta M^{\sigma}_{kk'}/M^{\sigma}_{kk'}) = \epsilon(\eta^2+1)^{1/2} \tag{4.6a}$$

where

$$\epsilon = \pm 4mV'(G)\,\mathrm{sgn}(V(G))/\hbar^2 G \tag{4.6b}$$

is a dimensionless measure of the importance of the correction. The total point α^2F function is (recalling that $\eta = y\sin\chi$)

$$\lim_{\omega\to 0}\alpha^2F(\boldsymbol{k},\omega) = \lim_{\omega\to 0}\alpha^2F^{(0)}(\boldsymbol{k},\omega)[1+\epsilon(1+y^2\sin\chi_G)^{1/2}]^2 \tag{4.7}$$

where the superscript (0) denotes the uncorrected α^2F of equation (3.8). This is equivalent to the result derived by WB; equation (3.8) makes the result more explicit. For the orbit average we expand the square and obtain three integrals of the type encountered in section 3. The corrected $\alpha^2F(\Gamma,\omega)$ is given by equation (3.11) with $I_G^{(0)}$ replaced by $(I_G^{(0)} + 2\epsilon I_G^{(1)} + \epsilon^2 I_G^{(2)})$, and the $I_G^{(n)}$ given by equation (3.12) and table 1.

In order to interpolate through the $\omega \sim \Omega_1$ region, note first that the term quadratic in $V'(G)$ (the $\epsilon^2 I_G^{(2)}$ term) has a significant I-OPW counterpart to interpolate with, whereas the linear term does not. It seems appropriate, therefore, to absorb the linear term in the zeroth-order interpolation described in section 3. The only effect of this is to change the crossover parameter a of equation (3.14) to

$$a = 4\sin\chi_G[3\cos^2\chi_G(I_G^{(0)} + 2\epsilon I_G^{(1)})]^{-1}. \tag{4.8}$$

For the term quadratic in $V'(G)$ we parallel the treatment of the zeroth-order term in section 3. In this case, the frequency dependences at low, intermediate and high frequencies are ω^2, ω^3 and (ω^2 + constant), respectively. The intraband contribution near $\omega \sim \Omega_1$ is therefore the greater of the ω^2 and ω^3 forms, as shown in figure 7, and the formal expression (including the sum over all vertices of the orbit) is

$$\delta\alpha^2F(\Gamma,\omega) = \tfrac{2}{15}(8\pi^2\hbar\rho v_F c_T^5 Q_\Gamma)^{-1}\sum_G \mathrm{cosec}(2\chi_G)G^2[V'(G)]^2$$
$$\times\{\theta(\omega-\Omega_1)\min[\omega^3, p(\omega)] + \mathrm{med}[b\Omega_1\omega^2, \omega^3, p(\omega)]\} \tag{4.9}$$

where $\mathrm{med}(\alpha,\beta,\gamma)$ takes on the value of its median argument. Again it is understood that the min and med functions are averaged over the two values of Ω_2 associated with a particular vertex, if these are different. The lower intraband crossover frequency $b\Omega_1$ is determined by equating the low-frequency form (the $\epsilon^2 I_G^{(2)}$ term) with half of the high-frequency form (equation (4.4)), with the result

$$b = \tfrac{15}{4} I_G^{(2)} \sin\chi_G. \tag{4.10}$$

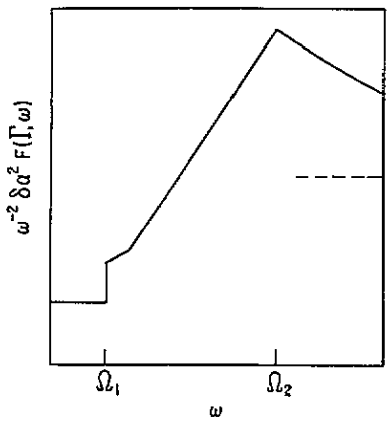

Figure 7. Corrections to $\alpha^2F(\Gamma,\omega)$ due to the momentum dependence of the form factor. Three regimes are evident as in figure 5. The broken line indicates the ω^2 asymptote at large ω.

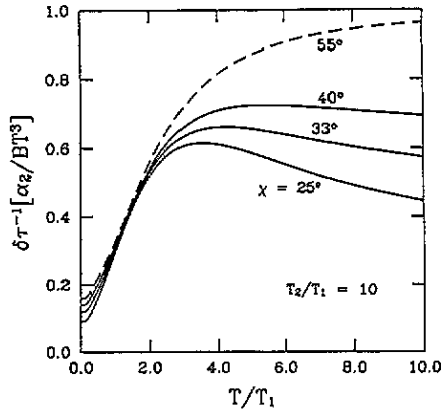

Figure 8. Correction to the scattering rate normalized to BT^3/α_2 (equation (4.11)). For $T > T_1$ the shape of these plots scales horizontally with T_2, which here is set to $10T_1$.

The resulting correction to the scattering rate, $\delta\tau^{-1}(\Gamma,T)$, is plotted in figure 8 for $T_2/T_1 = 10$ and several values of the vertex half-angle χ, which determines both α_2 and b (table 1), whose effects are seen at high and low temperatures, respectively. The high-temperature asymptotic behaviour to which this plot refers is

$$BT^3 \equiv \lim_{T_2\to 0} \delta\tau^{-1}(\Gamma,T) = \frac{56}{15\pi} N_G(8\hbar\rho v_F c_T^5 Q_\Gamma)^{-1}\mathrm{cosec}(2\chi_G)G^2 \times [V'(G)]^2\alpha_2\Omega_2(k_BT/\hbar)^3 \tag{4.11}$$

with the vertical axis scaled so that the curves approach a constant, α_2, at high temperatures. Full curves cover the expected range of values of χ (and α_2, table 1); the broken curve corresponds to $\alpha_2 = 1$ and is included only for reference. It is striking that an approximately T^3 dependence (arising from the large-ω behaviour of $\delta\alpha^2F$) persists down to $T \sim T_2/3$, well into the (nominal) intermediate regime.

The transient T^4-like behaviour seen at lower temperatures reflects the intermediate asymptotic form analogous to equation (3.15),

$$CT^4 \equiv \lim_{\substack{T_1\to 0\\ T_2\to\infty}} \delta\tau^{-1}(\Gamma,T) = \tfrac{2}{15}\pi^3 N_G(8\hbar\rho v_F c_T^5 Q_\Gamma)^{-1}\mathrm{cosec}(2\chi_G)G^2 \times [V'(G)]^2(k_BT/\hbar)^4 \tag{4.12}$$

where again N_G is the number of (assumed equivalent) vertices. The crossover between the approximate T^4 and T^3 behaviours may be located (at $\sim T_2/3$) by equating equations (4.11) and (4.12), ignoring the α_2 factor (whose effect is seen to be important only above this point) and recalling (equation (1.8)) that $\Omega_2 = k_BT_2/\hbar$. Moreover, as these formulae suggest, the overall shape of these curves, for $T \gtrsim T_1$, scales horizontally with T_2. This shape is determined by the cusp in $\delta\alpha^2F(\Gamma,\omega)$ at $\omega = \Omega_2$ (equation (4.9) and figure 7). The most crucial parameters governing $\delta\tau^{-1}$ are T_2 and the overall magnitude $[V'(G)]^2$.

5. Results

We are now in a position to ask under what conditions a T^2 contribution may be observable in the total scattering rate. A useful parameter for characterizing the importance of the contribution due to $V'(G)$ is the ratio R of the T^4 and T^2 asymptotic forms (equations (4.12) and (3.15)) evaluated at T_1:

$$R = \frac{\pi^2}{10}\left(\frac{V'(G)}{V(G)}\right)^2\left(\frac{k_B T_1}{\hbar c_T}\right)^2 = \frac{\pi^2}{10}\left(\frac{\epsilon}{\tan\chi}\right)^2 \tag{5.1}$$

where equations (1.7), (1.8) and (4.6*b*) were used to obtain the second expression. According to this definition the temperature T_x at which the two asymptotic forms would make equal contributions to the total rate τ^{-1} is

$$T_x = T_1 R^{-1/2}. \tag{5.2}$$

Since R is typically found between 0.1 and 0.2†, T_x is roughly double to triple T_1. This suggests that the $V'(G)$ contribution will almost always be significant in the regime where T^2 dependence is expected. It also suggests that if $T_2 \lesssim 3T_x$ this contribution will appear to be predominantly cubic, since the crossover from T^4 to T^3 dependence will then occur at or below T_x.

The total scattering rate, computed from equation (1.1) using the corrected α^2F (the sum of equations (3.13) and (4.9)), is plotted in figures 9(*a*)–(*d*). Uncorrected results corresponding to $R = 0$, similar to those of figure 6, are shown as broken curves. Values of both R and the vertex half-angle χ represent the range of values likely to be found in the simple metals†. The value of χ determines the other geometrical parameters a, b and α_2 (table 1), of which only α_2 has a large effect for $T > T_1$. The values of T_2/T_1, which can vary more widely, are chosen to indicate the range over which a T^2-like contribution is apparent.

The most surprising result is the robustness of an apparent T^2-like contribution outside of its expected regime ($T_1 < T < T_2$) when T_2/T_1 is not very large. There is a wide range of parameters where τ^{-1} appears to be a combination of approximate T^2 and T^3 dependences over a significant temperature interval above T_1. The apparent T^2 contribution may be identified as the intercept obtained by extrapolating to $T = 0$ the linear portion of the curve (if it exists) beginning slightly above T_1. This intercept is sometimes close to the ideal one (unity on these plots) and sometimes less. Both the magnitude and temperature range of the apparent T^2 contribution are helped by large T_2/T_1 when R is very small, and not so large T_2/T_1 when R is in the range 0.1–0.2, as is more likely the case.

The strength of the cubic contribution (the slope of the curves in figure 9) is proportional to both R and the ratio T_2/T_1. This may be understood simply by forming the ratio of asymptotic forms given by equations (4.11) and (3.15):

$$\frac{BT}{A} = \frac{28\alpha_2}{\pi^4} R\left(\frac{T_2}{T_1}\right)\left(\frac{T}{T_1}\right). \tag{5.3}$$

The negative curvature associated with smaller values of χ (or α_2) simply reflects the negative slope seen in figure 8 for $T \gtrsim T_2/3$. The transitional T^4 dependence of

† Representative of orbits found in Al, In, Cd and Mg.

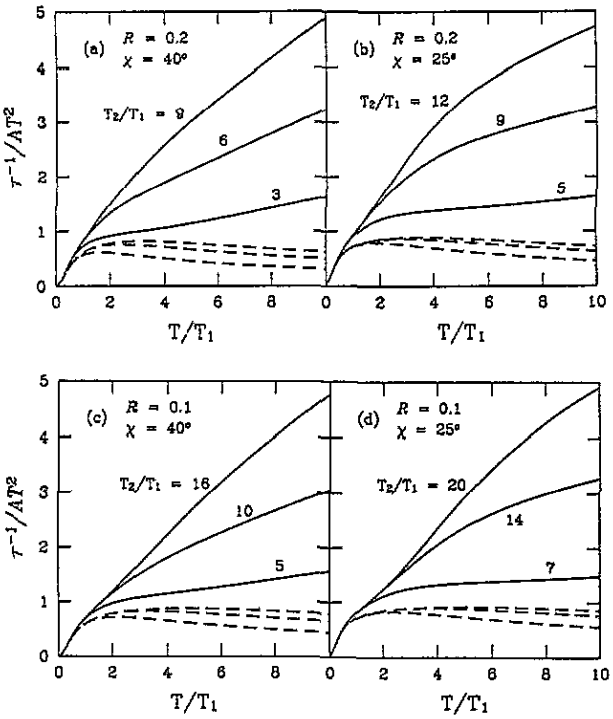

Figure 9. (*a*)–(*d*) Total scattering rate normalized to AT^2 (equation (3.15)) shows a variety of non-cubic behaviour for $T > T_1$. Within the expected range of parameters $R \leqslant 0.2$ and $25° \leqslant \chi \leqslant 40°$, there is a considerable range of T_2/T_1 values for which a T^2 contribution is apparent above T_1. Broken curves correspond to $R = 0$.

$\delta\tau^{-1}$ expected for $T \lesssim T_2/3$ is evident in figure 9 in the form of positive curvature only for small R and very large T_2/T_1.

An important point regarding the experimental observation of non-cubic temperature dependence stems from the fact that τ^{-1} can be resolved (using RFSE or surface Landau level resonance (SLL) techniques) typically only up to about 5–10% of the Debye temperature Θ_D. So one may not actually be able to explore the $T \gtrsim T_1$ regime in many orbits, since this would seem to require $T_1 \lesssim \Theta_D/50$. In contrast, the $T < T_1$ regime will be accessible on most if not all orbits studied. In this regime, the present model predicts a possible exponential behaviour in addition to the cubic, as shown in figure 6(*b*). An example of this is provided by Cd (Jaquier *et al* 1991), in which both regimes have been observed for orbits on the first and second zones, but only $T < T_1$ for third-zone orbits.

5.1. Further corrections

The importance of the contribution from $V'(G)$ seen in figure 9 raises the question why it is sufficient to treat the momentum dependence of the pseudopotential form factor $V(q)$ by a Taylor expansion about $q = G$ to only first order, as was done in equation (4.1). This may be addressed by showing that the next term, involving $V''(G)$, is unimportant for temperatures not too far above T_1. The reason for this is that

$$|V(G)| \ll Q_D|V'(G)| \sim Q_D^2|V''(G)| \tag{5.4}$$

(since G typically lies close to the zero of $V(q)$, where $|V'(q)|$ is relatively large)†. So temperature-dependent corrections entering with $[V''(G)]^2$ occur on the scale of Θ_D, while those with $[V'(G)]^2$ occur on the much smaller scale $T_x \sim T_1$ as seen above. The only remaining potentially important effect of $V''(G)$ is to change the magnitude (not the temperature dependence) of the correction associated with $[V'(G)]^2$. This occurs through a cross-term in the generalized equation (4.1), whose effect on final results (equations (4.9), (4.11) and (4.12)) may be expressed through the replacement

$$[V'(G)]^2 \rightarrow [V'(G)]^2 + 2V(G)V''(G). \tag{5.5}$$

This correction could become important if $|V'(G)|$ happened to be very small.

Other corrections to the temperature dependence of τ^{-1} arise from phonon dispersion (i.e. departures from the generalized Debye model used here) and of course the Debye cut-off. Although the latter could be incorporated trivially in the present model, its effect is negligible at temperatures where τ^{-1} can be resolved experimentally.

6. Conclusions

The foregoing results (summarized by equations (1.1), (3.13) and (4.9) as illustrated by figure 9) should be useful for predicting or interpreting both experimental data and full microscopic theoretical calculations. It seems clear from figure 9 that comparing experimental data with these results (which in principle have no adjustable parameters) can be much more informative than fitting to power laws or to polynomial forms such as $A_0 + A_2T^2 + A_3T^3$, where the interpretation may be ambiguous (see particularly the discussion in section 1 and Jaquier *et al* (1991)). Specific applications of this formalism have been made in Cd by Lawrence *et al* (1986) and by Jaquier *et al* (1991). A microscopic calculation for Cd by Chen *et al* (1992) confirms the existence of the T^2 regime predicted for orbital averages, in addition to a T^3 contribution. Applications to Al for both points and orbit averages will be reported later in this journal.

Acknowledgments

I would like to thank Robert Huguenin, Vitali Gasparov, Mike MacInnes, Pierre-Alain Probst and Rene Stubi for many conversations on quasiparticle lifetimes and the radiofrequency size effect, and James Swihart and Wei Chen for a fruitful collaboration on cadmium. This work was supported in part by the DOE–Basic Energy Sciences, Division of Materials Research.

† These conditions are verified in the cases mentioned. Only the smallest $|V(G)|$, which easily satisfy the first condition, admit experimentally observable regimes $T > T_1$ where momentum dependence of $V(q)$ is most important.

References

Allen P B and Silberglitt R 1974 *Phys. Rev.* B **9** 4733
Chen Wei, Swihart J C and Lawrence W E to be submitted to *J. Phys.: Condens. Matter*
Gasparov V and Huguenin R 1992 submitted to *Adv. Phys.*
Grimvall G 1976 *Phys. Scr.* **14** 63
Jaquier A, Probst P A, Stubi R, Huguenin R and Lawrence W E 1991 *J. Phys.: Condens. Matter* **3** 10 065
Lawrence W E, Chen Wei and Swihart J C 1986 *J. Phys. F: Met. Phys.* **16** L49
Lawrence W E and Wilkins J W 1972 *Phys. Rev.* B **6** 4466
Pickett W E 1989 *Rev. Mod. Phys.* **61** (2) 433
Probst P-A, MacInnes W M and Huguenin R 1980 *J. Low Temp. Phys.* **41** 115
Stubi R, Probst P-A, Huguenin R and Gasparov V A 1988 *J. Phys. F: Met. Phys.* **18** 1211
Wagner D K and Bowers R 1978 *Adv. Phys.* **27** 651